Nonequilibrium universality of Rydberg-excitation spreading on a dynamic network

Simon Ohler,[1] Daniel Brady,[1] Patrick Mischke,[1,2] Jana Bender,[1] Herwig Ott,[1] Thomas Niederprüm,[1] Winfried Ripken,[3,4] Johannes S. Otterbach,[5] and Michael Fleischhauer[1]

[1]*Department of Physics and Research Center OPTIMAS, Rheinland-Pfälzische Technische Universität Kaiserslautern-Landau, 67663 Kaiserslautern, Germany*

[2]*Max Planck Graduate Center with Johannes Gutenberg University Mainz (MPGC), 55128 Mainz, Germany*

[3]*Machine Learning Group, Technische Universität Berlin, 10587 Berlin, Germany*

[4]*Berlin Institute for the Foundations of Learning and Data, 10587 Berlin, Germany*

[5]*Orthogonal Otter UG, 10961 Berlin, Germany*

(Received 27 February 2025; accepted 13 July 2025; published 19 August 2025)

Understanding the universal properties of nonequilibrium phase transitions of spreading processes is a challenging problem. This applies in particular to irregular and dynamically varying networks. We here investigate an experimentally accessible model system for such processes, namely, the absorbing-state phase transition (ASPT) of Rydberg-excitation spreading, known as Rydberg facilitation, in a laser-driven gas of mobile atoms. It occurs on an irregular graph, set by the random atom positions in the gas, and, depending on temperature, changes its character from static to dynamic. By studying the behavior of the order parameter in the work of Brady *et al.* [Phys. Rev. Lett. **133**, 173401 (2024)], we showed numerical evidence for a crossover from directed percolation (DP) universality through various phases of anomalous directed percolation (ADP) to mean-field (MF) behavior when the temperature of the gas is increased. As the behavior of the order parameter is not sufficient to uniquely determine the universality class, we here analyze the distribution of avalanches—characteristic of nonequilibrium critical behavior—to fully characterize the ASPT. Performing extended numerical calculations and experiments on a cold ^{87}Rb atom gas, we confirm our earlier numerical findings and our phenomenological model that maps the dynamic network to a static one with power-law tails of the distribution of excitation distances. Furthermore, we discuss the influence of dissipation, present in the experiment and a necessary ingredient for the self-organization of the system to the critical point. In particular, we study the potential modification of the universality class by losses as a function of dissipation strength.

DOI: 10.1103/8rlg-169g

I. INTRODUCTION

The critical behavior at nonequilibrium phase transitions and the phenomenon of self-organized criticality (SOC) [1–3] are closely related to avalanche events—sudden, fast outbursts of energy after longer periods of inactivity. Although the topic is not without its controversies [4], the SOC mechanism is believed to be key to the abundance of real world examples of power-law distributed avalanche events like earthquakes [5], solar flares [6,7], and neuron activation in the brain [8,9], since it describes how a system can evolve in time to the critical point of a phase transition without an external drive or fine tuning. One of the most important categories of nonequilibrium phase transitions in spreading processes concerns absorbing-state phase transitions (ASPT). Here the behavior of the system changes from an active (spreading) phase with perpetual excitation cascades to an inactive (absorbing) phase, where a single excitation does not change the system at large. Power-law distributed avalanche events are then observed at the critical point between these two phases, reflecting the scale invariance of the critical state. In this situation, a minimal perturbation can cause a scale-free reaction of the system.

Avalanche events of self-organized critical systems have first been studied in the context of sandpile models, most notably the Bak-Tang-Wiesenfeld (BTW) model [1,2]. Shortly after, additional systems were proposed that display SOC behavior, such as the Manna [10], Drossel-Schwabl [11], or Olami-Feder-Christensen model (OFC) [12] for a different type of sandpile, forest fires, and earthquakes, respectively. Most of the avalanche research so far has focused on lattice models, where a toppling or relaxation event is defined as the transfer of, e.g., energy or particles to adjacent sites on the lattice. Some works have adapted these models to *networks*, where adjacency is not defined by nearest neighbors on the lattice but instead by links of the graph structure. Here, it was found that the type of graph structure itself can significantly affect the critical behavior [13].

Additionally, most work so far has been done on *static* systems, where the adjacency relations between individual sites do not change over time. This simplification is justified in many cases, since avalanches typically happen on very short timescales compared to other processes in the system.

However, in other systems, for example, epidemic spreading, the dynamical properties of the network are very important and happen on relevant timescales [14]. The extent to which graph dynamicity can impact the critical properties of the system is not well understood. In the context of the OFC model, for instance, it was found that the dissipative random-neighbor version results in noncritical behavior compared to critical scaling for fixed connectivity [15]; however, other authors claim that also in the latter case the model turns noncritical [16].

Generally, nonequilibrium phase transitions can be associated with a set of critical exponents that describe the scaling of physical observables close to the critical point. For ASPTs, these critical exponents can be related to the exponents of the power-law distributions of avalanche events [17]. Obtaining these critical exponents through experiments or simulations is essential to identify the universality class of the ASPT and can help in understanding the relevant physical processes.

For certain ASPTs, however, finding experimental representations can be very difficult. One example is the well-known universality class *directed percolation* (DP), where to this day well-controllable experimental systems are rare, the first one only being discovered in 2007 [18].

Gases of Rydberg atoms offer a versatile experimental platform for the investigation of many-body phenomena, where high-precision measurements on gases as well as on tailored geometries can be performed [19–21]. Interactions of Rydberg atoms can also be tuned to simulate the dynamics of the SIS (susceptible-infected-susceptible) model [22,23], which is an important example of a spreading model displaying an absorbing-state phase transition, and Rydberg atoms have been used experimentally to measure avalanche distributions and other critical exponents [24]. In this context, the excitation of an atom into a highly excited (Rydberg) state that can spread to other atoms is considered the "active" or infected state, whereas the ground state of the atom is the "passive" or susceptible state.

Absorbing-state phase transitions and DP universality of ensembles of Rydberg atoms have been previously studied on fixed lattices, yielding numerical [25] and experimental [26] signatures of DP in a one-dimensional chain of atoms. Additionally, cluster growth processes have been studied in a similar fashion [27]. In general, however, the spreading of an excitation occurs on a *network* of atoms with fixed spatial separation, given by the so-called facilitation distance. This network can be a regular lattice, if the atoms are trapped, e.g., in optical lattice potentials or tweezer arrays, or can be static but random, e.g., in a cold gas. An important further aspect of atomic gases is their thermal *motion*. In a recent publication we provided numerical evidence that the ASPT of a driven Rydberg gas under facilitation conditions changes its universality class as a function of the (root mean square) gas velocity [28]. For low temperatures we obtained DP scaling, changing to anomalous DP (ADP) and eventually mean-field (MF) for higher temperatures. These simulation results explained the unusual experimental measurement value of the critical exponent β obtained in a previous publication [24]. However, the change in universality was only shown for the critical exponent β as well as for one of the correlation length exponents $\nu_\parallel$ [28], lacking the third critical exponent $\nu_\perp$. Determining the exponents of the avalanche distribution functions at the critical point provides an alternative way to unambiguously determine the universality class, and we will pursue this approach in the present paper, by both numerical simulations and experimental studies. In addition, the scaling of avalanche critical exponents on dynamical networks such as in Rydberg facilitation remains a mostly open question, with only one exponent having been measured in Ref. [24].

In this paper, we numerically study the avalanche events in a three-dimensional gas of atoms that are driven by an external laser field and compare the results with experimental data as well as field-theoretical predictions for an effective static model with temperature-dependent power-law tails in the excitation distance. The atomic cloud is characterized by a tunable velocity distribution that, combined with the distance-dependent interaction, yields a dynamical graph on which excitations can spread. As a function of velocity we obtain the avalanche-exponents for area, size, and time of the avalanches (for a definition see Sec. III B) and confirm the universality class crossover from DP to anomalous directed percolation that we found in a previous publication [28] analyzing the β exponent of the order parameter, i.e., the Rydberg density. This is a nontrivial result since predicting the avalanche exponents requires knowledge of all three ASPT critical exponents (β, $\nu_\parallel$, $\nu_\perp$). The numerical results are supported by experimental observations of avalanche distributions of Rydberg facilitation in a cold, trapped gas of ^{87}Rb atoms. With this, our work also provides the first experimental indication consistent with ADP universality.

Secondly, the loss mechanisms inherent to self-organization of a system to the critical point of an absorbing-state phase transition can affect the universal behavior at criticality or even destroy criticality altogether. For this reason we consider additionally the effect of losses from the excited state and quantify its influence on criticality and exponent values for a frozen gas as well as a finite-temperature gas by numerical simulations. This is especially relevant in the context of our experimental results that invariably include loss.

II. RYDBERG FACILITATION, MODEL, AND EXPERIMENTAL SETUP

A. Microscopic system

We study a driven-dissipative system of atoms in three dimensions, where any atom can at any time belong to one of three states, namely, the ground state $|G\rangle$, the Rydberg state $|R\rangle$, and the "removed" state $|0\rangle$, which describes a state in which the atom does not take part in the dynamics at all (often called "immune" in the context of epidemic spreading). We apply an external driving (laser field) with Rabi frequency Ω that couples $|G\rangle$ to $|R\rangle$ with detuning Δ (see Fig. 1). The Rydberg state can spontaneously decay to the ground state with rate $(1-b)\gamma$ with $0 \leqslant b \leqslant 1$. The quantum mechanical evolution of the system can then be described by a Lindblad master equation [29] for the density operator $\hat{\rho}$, which reads (we set $\hbar = 1$)

$$\frac{\mathrm{d}}{\mathrm{d}t}\hat{\rho} = i[\hat{\rho}, \hat{\mathcal{H}}] + \sum_l \left(\hat{L}_l \hat{\rho} \hat{L}_l^\dagger - \frac{1}{2}\{\hat{L}_l^\dagger \hat{L}_l, \hat{\rho}\} \right), \qquad (1)$$

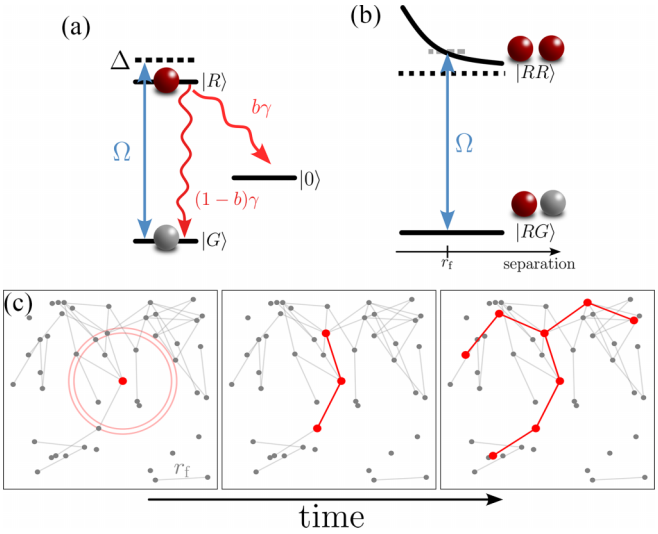

FIG. 1. Overview over the microscopic physics in our model. (a) Single atom under external drive Ω with decay channels into ground and inactive states. The parameter b controls the ratio between the decay processes. (b) Two atoms with interatomic van der Waals force that shifts the two-Rydberg state as a function of distance. At $r = r_f$, the shift cancels the external detuning and the transition becomes resonant. (c) Spreading of an avalanche on a network.

where the unitary evolution of the system is given by

$$\hat{H} = \sum_i \Omega\hat{\sigma}_i^x - \Delta\hat{n}_i + \sum_{j<i} \frac{c_6}{r_{ij}^6}\hat{n}_i\hat{n}_j. \tag{2}$$

Here, $\hat{n}_i = (|R\rangle\langle R|)_i$ is the number operator of the Rydberg $|R\rangle$ state, $r_{ij} = |\vec{r}_i - \vec{r}_j|$ is the interatomic distance, and $\hat{\sigma}^x$ is the Pauli x matrix. The last term in (2) corresponds to the van der Waals interaction between two Rydberg atoms with c_6 being the van der Waals coefficient. Using the Lindblad master equation, the dissipation in the system is taken into account by the Lindblad jump operators $\hat{L}_1^{(i)} = \sqrt{(1-b)\gamma}\,(|G\rangle\langle R|)_i$, $\hat{L}_2^{(i)} = \sqrt{b\gamma}\,(|0\rangle\langle R|)_i$, which describe spontaneous decay of the $i'th$ atom from the Rydberg state into the ground state $|G\rangle$ and the inert state $|0\rangle$, respectively, with the branching parameter b. Additionally, we include the effect of dephasing, which stems mainly from laser phase noise and Doppler broadening [24], but also from the nonzero width of the wave function of the atom over the van der Waals potential [30], and differential van der Waals forces [31]. The dephasing Lindblad operator reads $\hat{L}_\perp^{(i)} = \sqrt{\gamma_\perp}\hat{n}_i$, where $\gamma_\perp$ is the dephasing rate.

In this publication, we always consider the high-dephasing limit of the Rydberg gas, which has been proven to be a good approximation for gaseous Rydberg systems [32]. In this limit, the dynamics of the system is governed by effective rate equations, which can be modeled using a classical Monte Carlo approach [33] (for more details see Appendix A).

B. Facilitation mechanism

The level scheme of a single Rydberg atom and the two-Rydberg dynamics is illustrated in Fig. 1. In the *facilitation* regime, the detuning Δ is chosen sufficiently large to suppress spontaneous (seed) excitations from the ground state. However, if one atom in the system is initially in the Rydberg state, then the van der Waals interaction shifts the Rydberg energy levels of the nearby ground-state atoms. Since the van der Waals interaction is distance dependent, there exists a distance called the *facilitation radius* $r_f = (c_6/\Delta)^{1/6}$, at which the van der Waals interaction exactly cancels the detuning. In this way, a Rydberg atom can resonantly "pass on" the excitation to other atoms in a spherical shell with radius r_f around it. The width of this shell δr_f is given by $\delta r_f = \frac{\gamma_\perp}{2\Delta} r_f$ with $\delta r_f / r_f \ll 1$ [34]. The rate of the resonant facilitation is denoted by $\Gamma_f = 2\Omega^2/\gamma_\perp$, which is an important timescale in the system. Combining these two effects, we see that while an initial (seed) excitation is very unlikely, as soon as Rydberg atoms exist in the system it is possible to observe avalanche-like cascades of excitations. For this a sufficiently high density and strong enough external driving is needed such that the global facilitation rate is stronger than the decay from the Rydberg state to the ground state. At high atom velocities, the Rydberg atoms see a homogeneous ground-state background and the number of facilitated excitations is determined by the density and driving strength only. For a frozen gas with velocity $v = 0$, however, the atoms form a network where two atoms are connected if and only if their distance falls into the very narrow interval $r_f \pm \delta r_f$. Since the atomic positions are distributed uniformly, the resulting network of atoms that in principle can participate in the Rydberg facilitation is of the Erdős-Rényi [35] type [34].

C. Rydberg gas as a dynamical graph

The Erdős-Rényi network for the frozen gas is characterized by a Poissonian distribution P_{ER} of the number k of atoms in the facilitation shell of a single Rydberg atom,

$$P_{ER}(k) = \frac{(nV_s)^k}{k!}\exp(-nV_s). \tag{3}$$

Here, $V_s \approx 4\pi\delta r_f r_f^2$ is the volume of the facilitation shell and $n = n_G + n_R$ the total density of remaining atoms in the ground and Rydberg states. It is well known that such a network features a percolation transition at the average network degree $\langle k\rangle = 1$. To be able to observe universal behavior, the network needs to be above this threshold, since otherwise the system is comprised of disconnected, finite clusters [34] and a universal data collapse cannot be achieved [28]. Therefore, the average degree $\langle k\rangle = nV_s$ needs to be sufficiently larger than unity. To increase $\langle k\rangle$ in our simulations we increase n; however, that comes with significantly increased computational cost, leading us to choose $\langle k\rangle \sim 2.5$ as a reasonable compromise. For this value, approximately 90% of atoms are contained in the largest connected cluster (LCC) of atoms that in principle could undergo Rydberg facilitation. For finite temperature, the system has to be represented as a dynamical graph, since the distances between the atoms change over time. This implies that the pairs of atoms between which an excitation can spread (pairs of atoms with a mutual distance close to r_f) change over time, which, in the language of graph theory, corresponds to the creation and desctruction of links between nodes. Changing the gas velocity then allows to change the rate of link creation and destruction and therefore

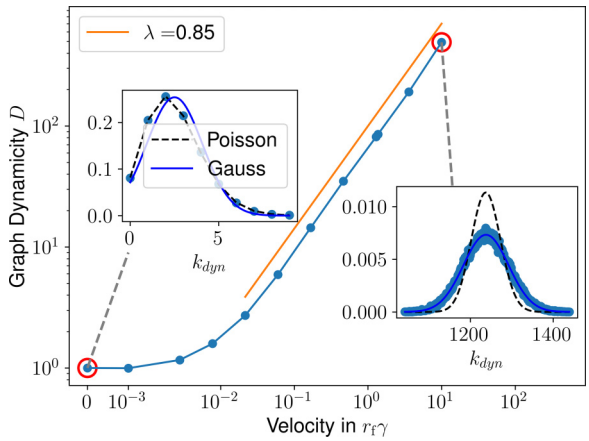

FIG. 2. Average number of unique links an atom encounters over the time $1/\gamma$ as a function of rms velocity normalized to the $v = 0$ case. The insets show the full distribution for velocities $v = 0$ (left) and $v = 10 r_f \gamma$ (right) as well as Poissonian and Gaussian fits.

the degree to which dynamical effects become relevant. We quantify the degree to which the graph is dynamical by introducing the graph dynamicity D, which reads

$$D = \frac{\langle k \rangle_{\text{dyn}}}{\langle k \rangle_{\text{stat}}}, \tag{4}$$

where k_{dyn} counts all unique atoms (nodes) that an atom has ever been connected to during the inverse decay time $1/\gamma$ and k_{stat} is the average number of instantaneous connections (determined fully by the density and width of the facilitation shell). The result can be seen in Fig. 2. We observe that after a period of slow growth, starting from $v \sim 0.02 r_f \gamma$ we see a continuous power-law increase in the number of unique connections. Additionally, at this point the distribution of unique partners changes from Poissonian (low-velocity) to Gaussian (high-velocity). Coincidentally, this velocity scale agrees well with the upper limit of DP universality found in Ref. [28]. In addition to the data, we also show the power-law fit to the velocity interval from $v > 0.06 r_f \gamma$, which yields the exponent $\lambda = 0.85$. The relevance of this power-law increase in dynamicity is, however, unclear. We note that this consideration takes into account solely the dynamical graph structure of atoms on which Rydberg facilitation is in principle possible, not the actual excitation dynamics that depends on other factors like the external drive intensity.

D. Experimental setup

To experimentally study the collective Rydberg facilitation dynamics, we prepare a cloud of ^{87}Rb atoms in a crossed optical dipole trap with trapping frequencies of $\omega_{x,y,z} = 2\pi \times (332, 332, 73)$ Hz. The experimental setup is sketched in Fig. 3. Forced evaporation in the dipole trap is stopped at a final temperature of $T = 1\,\mu$K, leading to a thermal cloud with a density of $\rho = 2.2 \times 10^{13}\,\text{cm}^{-3}$. This temperature corresponds to an rms velocity of $v = 0.39 \pm 0.26 r_f \gamma$. The facilitation dynamics is induced by off-resonant, blue-detuned ($\Delta = 40$ MHz), continuous excitation from the $|G\rangle \equiv |5S_{1/2}\, F = 2\, m_F = 2\rangle$ ground state to the $|R\rangle \equiv |40P_{3/2}\rangle$ Rydberg state for a total duration of 100 ms. Due to

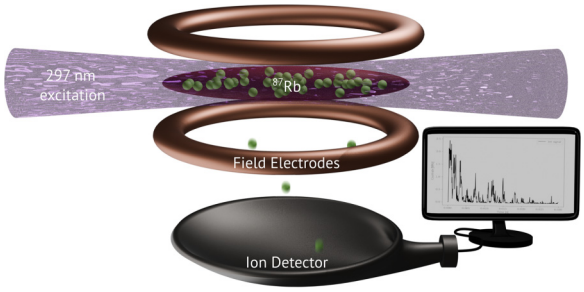

FIG. 3. Sketch of the experimental setup. The Rydberg laser off-resonantly drives facilitation dynamics and cascades of Rydberg excitations (green circles) appear in the cold cloud. Rydberg atoms can decay into ions via photo- or associative ionization, which are guided to an ion detector where their arrival time is recorded. This allows to observe the facilitation dynamics continuous in time.

photoionization from the dipole trap lasers and associative ionization, a fraction of the Rydberg population gets ionized. This decay channel contributes to the dissipation process that brings atoms into the inactive state $|0\rangle$. This state accounts for ions, atoms lost from the system since the Rydberg state is not trapped, and also atoms that decayed to the $|5S_1/2\, F = 1\rangle$ ground state, which does not participate in the excitation dynamics. We estimate that approximately 2/3 of the Rydberg excitations decay back to the $|G\rangle$ state, i.e., the branching ratio is $b \approx 0.3 \pm 0.15$. The created ions are accelerated through a small electric field toward an ion detector, where their arrival time is detected. In this way, we obtain a time-continuous measurement signal proportional to the Rydberg density, which allows the observation of the facilitation dynamics *in situ*. Due to the discrete nature of the ion arrival information, binning the data is required to obtain an ion rate.

III. UNIVERSALITY CLASS AND AVALANCHE DISTRIBUTION

A. Crossover of universality classes in Rydberg facilitation

In Ref. [28], it was shown by extensive numerical simulations that the absorbing-state phase transition in a Rydberg gas changes its universality class from DP through ADP to MF by varying the velocity of the atoms. This crossover was explained by mapping the Rydberg facilitation dynamics on the dynamic network to a spreading process on a fixed network, however with long-distance power-law tails in the distribution of excitation distances. The power-law tails in the probability distribution of distances between excitations emerge since, due to the finite temperature of the gas, excited Rydberg atoms can move larger distances before actually exciting another ground-state atom. In order to determine the probability distribution of distances r a Rydberg atom needs to move before facilitating another atom, the space covered by the Rydberg atom is discretized, i.e., $r = J\delta z$ with $J \in \mathbb{N}$ [28]. This probability reads $Q(X > J) = (1 - p_{\text{exc}})^J$, where p_{exc} is the excitation probability in a given discretized interval δz. In particular, if the Rydberg atom moves at velocity v, the time spent in δz is given by $\delta t = \delta z / v$. For a single atom the excitation probability in this interval δt is Poissonian and reads $p_\uparrow = 1 - \text{e}^{-\Gamma_f \delta t}$. Furthermore, the number of atoms in

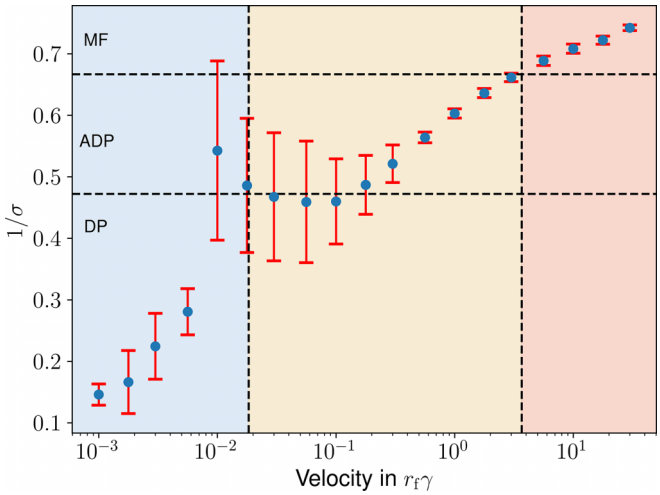

FIG. 4. Reciprocal Lévy-flight parameter as a function of gas velocity. The horizontal lines denoting the transition from one universality class to another are given by Ref. [17]. The vertical lines correspond to the velocities $v_- = \delta r_f \Gamma_f$ and $v_+ = r_f \Gamma_f$. Shown data has also been presented in Ref. [28].

the facilitation shell of a Rydberg atom also follows a Poissonian distribution and therefore the excitation probability reads $p_{\text{exc}} = \sum_{k=0}^{\infty} P(k)(1-(1-p_\uparrow)^k)$, i.e.,

$$p_{\text{exc}} = 1 - \exp\{-\xi \delta z\}, \tag{5}$$

with $\xi = \frac{\langle k \rangle}{\delta r_f}(1 - e^{-\delta r_f \Gamma_f / v})$. This then yields the probability distribution of distances r from the initial position of the Rydberg atom for the first successive excitation

$$Q(r) = 2\pi \xi r \int_0^\pi d\theta \, \frac{e^{-\xi(\sqrt{\cos^2\theta + r^2 - 1} - \cos\theta)}}{\sqrt{\cos^2\theta + r^2 - 1}}, \tag{6}$$

where $\vec{r} = r_f \hat{e}_r(\theta, \varphi) + (0, 0, z)^T$. We have shown in Ref. [28] that this distribution agrees very well with the numerically obtained distribution of first excitations in the finite-temperature gas. It also agrees very well with a power-law fit of the form

$$P_{\text{hop}}(r) \sim \frac{1}{r^{d+\sigma}}, \tag{7}$$

which resembles a Lévy-flight statistic for d being the dimension of space and σ the Lévy-flight parameter.

In Fig. 4 we show the inverse Lévy-flight parameter over the gas velocity $1/\sigma$, obtained from power-law fits to the distances between excitations in the simulated gas [28]. We see that the Lévy-flight parameter $\sigma = \sigma(\bar{v})$ depends on the average velocity $\bar{v} = (\langle v^2 \rangle)^{1/2}$ of the atoms, causing a transition between universality classes. The critical exponents $(\beta, \nu_\parallel, \nu_\perp)$ characterizing the behavior of the order parameter (Rydberg density), temporal, and spatial correlations, respectively, can be approximated as a function of σ close to the MF regime via a renormalization-group approach. In this case, for $d = 2\sigma - \epsilon$, ϵ being a small parameter representing the distance to the upper critical dimension, the exponents can be written as [36]

$$\begin{aligned} \beta &= 1 - \frac{2\epsilon}{7\sigma} + O(\epsilon^2), \\ \nu_\perp &= \frac{1}{\sigma} + \frac{2\epsilon}{7\sigma^2} + O(\epsilon^2), \\ \nu_\parallel &= 1 + \frac{\epsilon}{7\sigma} + O(\epsilon^2). \end{aligned} \tag{8}$$

In Ref. [28] we determined two of the three critical exponents β and $\nu_\parallel$, characterizing the order parameter and temporal correlations, while the third one, $\nu_\perp$, which determines spatial correlations, was not accessible. In the following we discuss an alternative approach to fully determine the universality class, which we pursue in this work, both numerically and experimentally.

B. Avalanches

A characteristic phenomenon in dynamical systems close to the critical point of an ASPT is the appearance of avalanches, i.e., cascades of excitation events spreading through the system. Their time t (duration), area a, and size s are random but show a power-law probability distribution, which reflects the scale invariance at the critical point. For the definitions of area and size we follow Ref. [17], where the area is the number of unique sites (in our case atoms) that were involved in the avalanche, while size is the total number of relaxation (in our case decay) events that took place in the avalanche, counting possibly multiple relaxations for a single atom. Time is measured from the first excitation to the last decay of the avalanche. The distributions then scale as

$$P(t) \sim t^{-\tau_t}, \quad P(s) \sim s^{-\tau_s}, \quad P(a) \sim a^{-\tau_a}. \tag{9}$$

Generally, the critical exponents of the ASPT $(\beta, \nu_\parallel, \nu_\perp)$ are connected to these avalanche exponents in the following way [17]:

$$\tau_a = 1 + \frac{\beta}{d\nu_\perp}, \quad \tau_s = 1 + \frac{\beta}{\nu_\parallel + d\nu_\perp - \beta}, \quad \tau_t = 1 + \frac{\beta}{\nu_\parallel}. \tag{10}$$

For the MF case, the critical exponents $\beta, \nu_\perp, \nu_\parallel$ are known exactly, while for DP there exist numerical estimates in the literature [37]. For the case of ADP, the critical scaling of the system depends on the Lévy-flight parameter $\sigma = \sigma(\bar{v})$.

1. Simulation results

To numerically investigate the critical properties at the boundary between absorbing and active phase in the Rydberg gas, we first need to pinpoint the parameters to obtain the critical state, namely, the critical driving-strength parameter Ω_c and the corresponding critical density n_c. To see universal scaling in our system, the underlying Erdős-Rényi network needs to be well above the percolation threshold [34], so we fix $n_c = 20.0 r_f^{-3}$, which corresponds to an average network degree of $\langle k \rangle = 2.5$. This holds for all gas velocities that we consider, while Ω_c changes as a function of velocity. We then determine the critical driving strength Ω_c via active-density decay, where we start with all atoms in the excited state and observe the decay process to the ground state ($b = 0$) (see

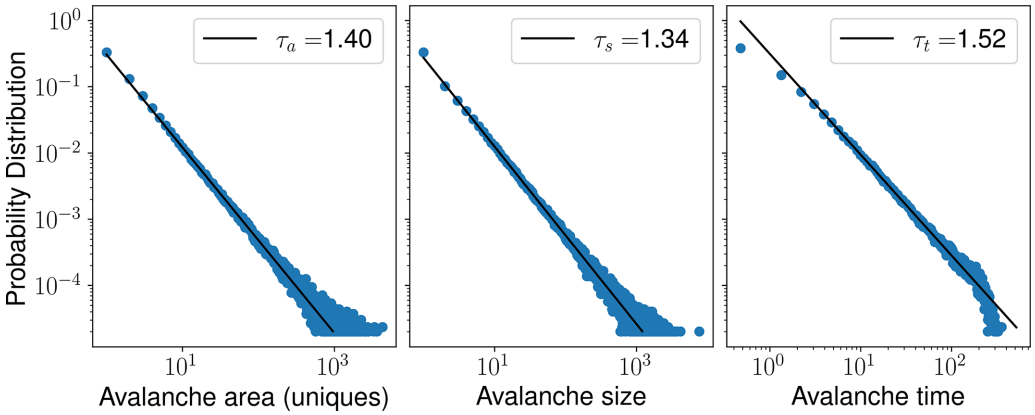

FIG. 5. Simulation avalanche area, size, and time distributions for $v = 0$ and a system size of $L = 20r_f$. The power-law fit function is shown in black. Note that statistically insignificant counts have been omitted. The broadening and drop in the distributions for large values are results of low statistics and finite-size effects.

also Appendix C). In the absorbing state, the active density ρ will decrease exponentially with time, for an active state ρ approaches a constant value, and for the critical state we expect power-law decay [34,38]. Note that we could simply use the SOC mechanism ($b \neq 0$) to obtain the critical state by starting in the active phase and time-evolving to the phase transition. However, to achieve sufficient accuracy this would necessitate an extreme separation of time scales, which is computationally more expensive.

Having obtained the critical parameters, we perform repeated calculations where we generate a gas of ground-state atoms at density $n = n_c$ and driving $\Omega = \Omega_c$. Furthermore, we use $\Delta/\gamma = 1000$, $\gamma_\perp/\gamma = 20$, and a cubic simulation volume with edge length L and periodic boundary conditions. During a simulation, we place a single excitation in the gas and let the system evolve until no excited atoms remain, extracting the area, size, and time of the avalanche. In this manner, we obtain approximately 10^5 avalanches for each configuration of parameters, allowing us to analyze the occurrence statistics. See Fig. 5 for example distributions for a fixed system size at $v = 0$. We do not extract the avalanche exponents from such distributions directly, but perform a finite-size expansion on the fitted exponents for system sizes up to $L = 20r_f$. For more details see Appendix B.

Using the two sets of equations, Eqs. (8) and (10), and the mapping $\sigma(v)$ from Ref. [28] (see Fig. 4), we can make predictions about the expected avalanche exponents τ_t, τ_a, τ_s over the Rydberg gas' velocity in the DP, ADP, and MF regimes. In Ref. [28] we additionally found that the Rydberg gas enters the ADP II phase in between DP and ADP, which is additionally characterized by Lévy-flight distributed waiting times between facilitation (infection) events [39]. For this regime, however, we cannot obtain theoretical predictions for the critical exponents.

In Fig. 6 we show the predictions in the DP, ADP, and MF phases combined with both the results of the simulations as well as the experimental data for the time and magnitude exponents. The experimental magnitude exponent corresponds to the area and size exponents; see the next section for details. For the DP values, the thickness of the bars indicate the uncertainty of the avalanche exponents derived from the uncertainty of the critical exponents ($\beta, \nu_\perp, \nu_\parallel$) in the literature. For the ADP values, the uncertainty interval is computed from the σ uncertainty as shown in Fig. 4. The ADP predictions for smaller velocities are shown with dashed lines and a shaded uncertainty area, since the position at which a crossover to the ADP II phase occurs is not known precisely. We observe that for the expected DP and ADP universality classes the simulation results agree very well with the literature values and the ADP values found in Ref. [28]. For the case of $v = 10r_f\gamma$ in the MF regime we see that while the time exponent remains close to theoretical predictions, the area and size exponents are larger than the expected long-range (LR) MF case.

There are two distinct MF cases that result in different area and size exponents, depending on the dimension and the range of interactions [17]. Short-range (SR) MF is expected for $d \geqslant 4$ and $\sigma \geqslant 2$ and is characterized by the critical exponent $\nu_\perp^{\mathrm{SR}} = 1/2$. In contrast, the LR MF case appears for arbitrary dimension as long as $\sigma < \min(2, d/2)$ and is associated with the value $\nu_\perp^{\mathrm{LR}} = 1/\sigma$. Our simulations give values of the area/size exponents that are in between the SR and LR mean-field predictions. We do not have an understanding for this behavior. However, it is important to note that both the SR-MF as well as the LR-MF literature values were obtained from static models on regular lattices, whereas we consider a dynamical graph. Obviously, the mapping of moving atoms with close-range interactions to a static network with long-range connections (Lévy flights) breaks down when the atom velocity becomes too large.

2. *Experimental results*

In order to observe the system at the critical point in the experiment, the gas is initialized with parameters for the density and driving strength such that the dynamics always starts in the active phase. Due to atom loss, as described above, the density and thus the effective driving strength are reduced and the system evolves toward the critical point (self-organization of criticality). In the vicinity of the critical point the detected ion signal distribution becomes clearly non-Poissonian and avalanches of various sizes can be observed. The atom loss rate is reduced as it scales with the Rydberg density. After reaching the critical point, the system evolves slowly away

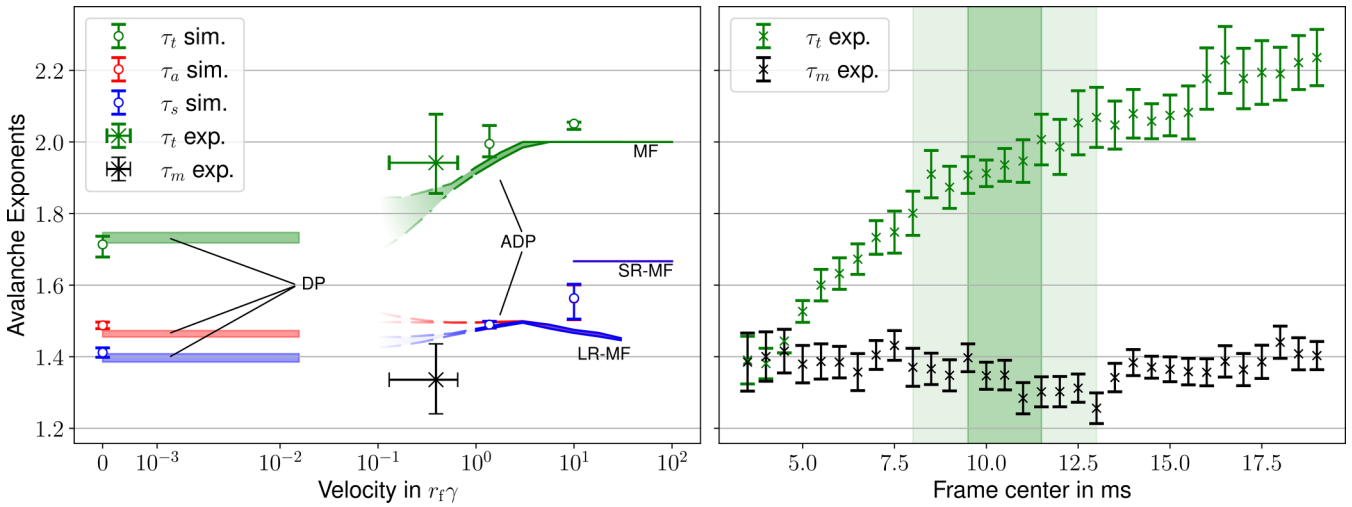

FIG. 6. Left plot: Simulation avalanche exponents over velocity (in units of $r_f\gamma$) for $b = 0$. Each velocity uses a different value of $\Omega = \Omega_c$. Note that for both mean-field cases, the theoretical predictions for area and size become identical. The perturbative ADP predictions fade out away from mean field. Also shown are the experimentally extracted values for time and magnitude (in the experiment area and size cannot be distinguished). For an explanation of the latter, see text. Experimental values are derived from the highlighted area in the right plot. Right plot: Experimental avalanche exponents as a function of time. Error bars represent the fit uncertainty; additional systematic errors may arise from, e.g., binning. The dark green area corresponds to our estimate for t_{crit}, at which the critical point of the ASPT is reached. For more details on the t_{crit} estimation see Appendix C.

from the critical point for two reasons. Firstly, the off-resonant driving laser continues to create excitations at a low rate even in the absorbing phase. Secondly, as long as there are Rydberg excitations present, atoms will continue to become ionized or decay into inert states. In the absorbing phase, the system, even though it is noncritical, still shows power-law scaling over finite scales. This dynamic in the measurement poses two challenges when extracting the critical avalanche exponents: (1) We need to find a reliable method to extract avalanches in a system where the starting and ending time of avalanches are masked by a random seed process, and (2) we have to estimate rather accurately where the critical point is reached during the time evolution of the sample. To distinguish different avalanches, we bin our data in $t_{\text{bin}} = 50\,\mu\text{s}$ intervals corresponding to the theoretical lifetime of the $40P_{3/2}$ Rydberg state and consider an avalanche to end and the next avalanche to start if one of those bins does not contain any counts. The duration of an avalanche is then given by the number of consecutive nonempty bins, and the magnitude of the avalanche is quantified by the number of events in those bins. It is not possible to count the number of times an atom gets excited to the Rydberg state and decays back to the ground state, and at the same time, not all atoms that have been excited end up ionized. Therefore, the experimental magnitude of an avalanche cannot be exactly mapped to either the area or size exponent, and we are unable to define an exact relation between the empirical τ_m and τ_a as well as τ_s. However, the difference in theoretical prediction between both exponents in the ADP regime is negligible compared to the experimental uncertainty.

When the system evolves from the active to the absorbing state, it eventually becomes critical. It is, however, not trivial to precisely determine at what time t_{crit} the critical point is reached, as can be seen by looking at the average ion count rate during the measurement shown in the left plot of Fig. 7. Starting in the active phase, we observe a steep drop in the signal 2 ms after the pulse started, corresponding to a rapid reduction in the number of facilitation partners due to loss into the inert state.

In contrast, after 15 ms the strongly reduced decay rate signals the absorbing phase where the decay is driven by the off-resonantly created seeds and the exponentially dying avalanches. The distribution of avalanche durations and magnitudes continues to follow a power law around the critical point as shown in Fig. 7. To account for the uncertainty in the precise time t_{crit} at which the critical point is reached, we analyze the avalanche exponents in three overlapping time windows of length $\Delta t_{\text{window}} = 3$ ms in the time range 3.5–14.5 ms. By fitting a power law to the avalanche occurrence statistics in the respective time window, we can extract the time and magnitude exponents for the avalanches. Since the power-law behavior prevails even away from the critical point, its presence alone cannot serve as an indicator for the time at which the system is critical. Instead, to estimate t_{crit}, we analyze the activity distribution in the corresponding time windows as detailed in Appendix C and obtain an estimate of $t_{\text{crit}} \approx 8 \ldots 13$ ms (light green in Fig. 6), i.e., centers of the overlapping evaluation windows ranging from 9.5 to 11.5 ms (dark green in Fig. 6).

In Fig. 6 we plot the results for the simulation along with the data extracted from the experiment. The horizontal error bars in the left plot denote the uncertainty regarding the lifetime of the Rydberg states. In the right plot, the continuously changing avalanche exponents are shown. Additional contributions to the uncertainty in the exponent values emerge from systematic sources such as the choice of t_{bin} and are not shown.

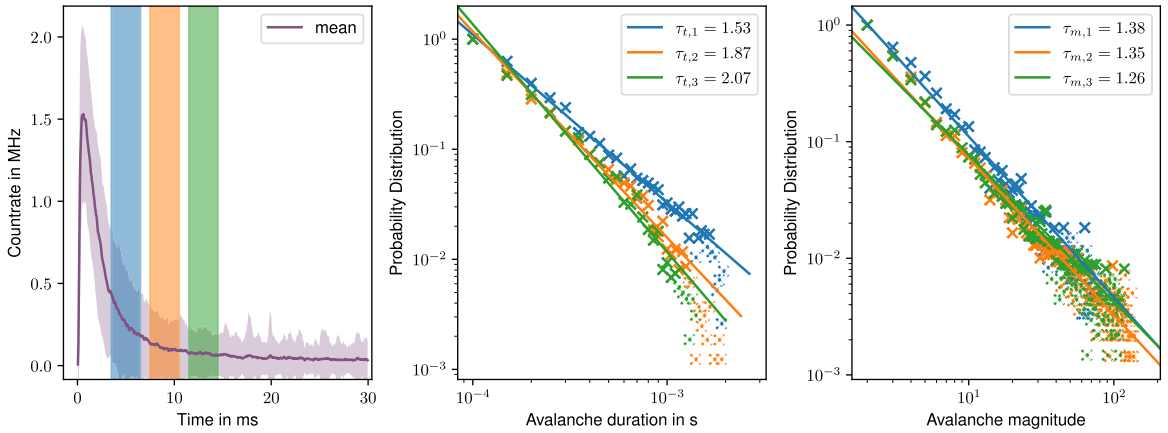

FIG. 7. (Left) Average ion countrate during the excitation pulse, averaged over 1000 realizations (purple). The dynamics starts in the active phase. The shaded purple area illustrates the standard deviation between runs. The colored vertical boxes show the $\Delta t_{\text{window}} = 3$ ms long time windows used to extract the avalanche exponents (centered at blue: 5 ms, orange: 9 ms, green: 13 ms). (Middle) Normalized distribution of (middle) avalanche durations and (right) avalanche magnitudes in the three different time windows (blue, orange, and green). Dashed data points have been ignored for fitting the power-law distribution.

We can see that the experimental time exponent for the critical interval falls into the ADP range and is clearly incompatible with the DP universality class. The magnitude exponent is smaller than expected for ADP universality, however it is unclear if this deviation might be caused by our measurement imperfections.

Additionally, the experimental data allows to exclude other, similar universality classes like the Manna class [10], where in three dimensions a time exponent of $\tau_t^{\text{Manna}} \approx 1.78$ is expected. We can also rule out that the Rydberg gas belongs in the BTW-class universality, as for that model a three-dimensional (3D) time exponent of $\tau_t \sim 0.92$ was predicted [2]. However, one should note that the two-dimensional (2D) predictions of said Ref. [2] are the subject of intense debate since no simple finite-size scaling seems to exist [17,40,41].

IV. INFLUENCE OF DISSIPATION

A. Effect of self-organization on Erdős-Rényi character of excitation graph

One important question is how the decay channel $b\gamma$ into the inert state $|0\rangle$, responsible for the self-organization of the facilitated Rydberg gas to the critical point, affects the properties of the network of possible excitations. As atoms in the inert state no longer interact with other atoms, we do not consider them as part of the graph. Furthermore since the decay into the inert state affects only atoms in the Rydberg state, it may lead preferentially to a loss of large clusters of atoms that are pairwise in facilitation distance. This could affect the structure of the network in particular for a frozen gas, where this network is a static Erdős-Rényi network. To analyze this effect, we calculate the degree distribution $P(k)$ for an initially percolating graph with loss parameter $b = 0.3 > 0$ (see Fig. 8).

By fitting with a Poissonian function, with fit parameter $\langle k \rangle$, we find that the degree distribution $P(k)$ remains Poissonian, albeit with a continuously changing average degree $\langle k \rangle$, plotted in the inset.

B. Effect of dissipation on the universality class

Dissipation is an essential ingredient of the SOC mechanism. It typically introduces characteristic length and time scales and thus strict scale invariance is lost. In the context of branching processes, for example, nonconservation of the particle number leads to a self-organization into an attractor state that is not critical but *subcritical*, leading to an exponentially truncated distribution of avalanches [42]. As a result, the distribution functions of avalanches no longer decay as a pure power law, but rather as

$$\begin{aligned} P(t) &\sim t^{-\tau_t}\, h_t(t/t_c), \\ P(s) &\sim s^{-\tau_s}\, h_s(s/s_c), \\ P(a) &\sim a^{-\tau_a}\, h_a(a/a_c), \end{aligned} \tag{11}$$

where the $h_\mu(x)$ are cutoff functions with cutoff scales x_c that grow with decreasing dissipation strength. Some authors have referred to this as *quasicriticality* [16]. It is also argued [16]

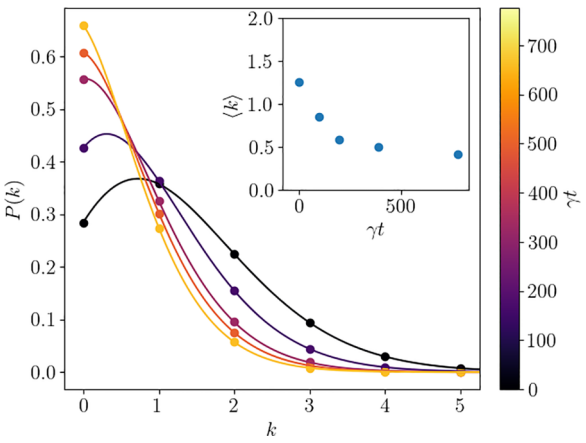

FIG. 8. Node degree distribution (dots) for different times in the frozen gas with loss parameter $b = 0.3$ and Poissonian fit with fit parameter $\langle k \rangle$ (solid lines). Fit parameter (average degree) $\langle k \rangle$ over time (inset).

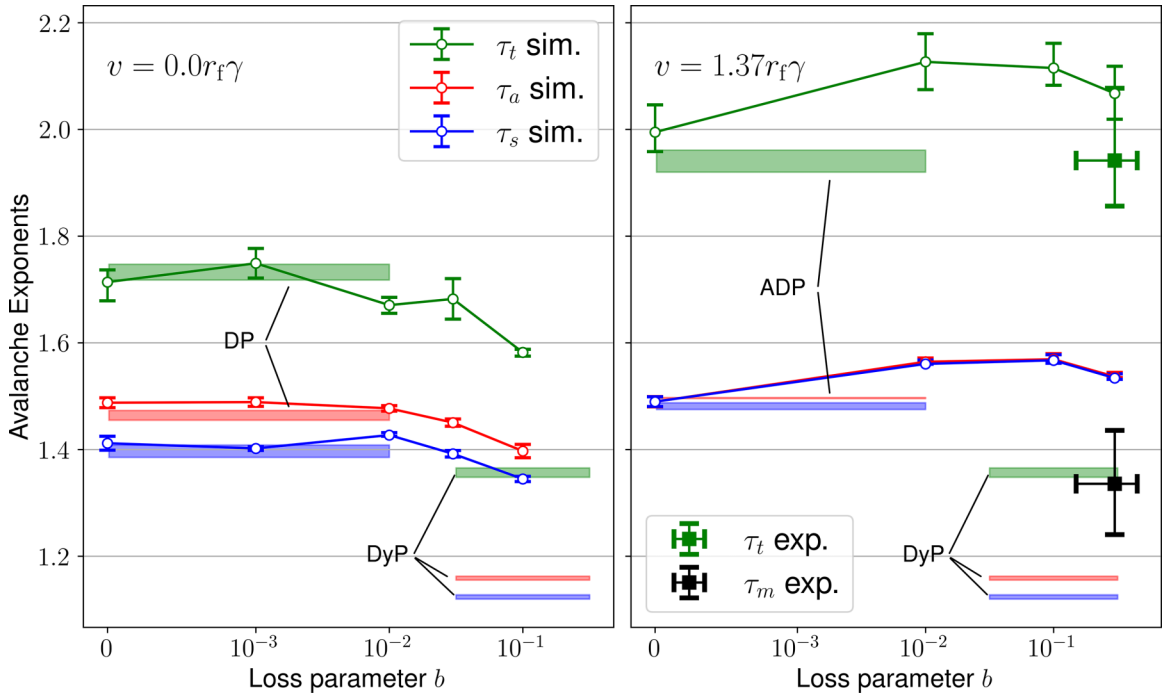

FIG. 9. Finite-size extrapolated avalanche exponents over loss parameter b, for the cases of $v = 0$ in the DP regime (left) and $v = 1.37 r_f \gamma$ for the ADP case (right). The red, blue, and green bars show the expected exponents of area, size, and time, respectively, for the universality class as stated. Note that in the case of the frozen gas for $b > 0.1$ the distributions of area, size, and time become increasingly characterized by an early exponential cutoff, resulting in a poor power-law fit, which is why we focus on $b < 0.1$. Importantly, for both velocity cases the exponents do not approach the values expected from the dynamical percolation (DyP) universality class.

that a "loading mechanism" can counteract the dissipation by replenishing the lost particles after each avalanche, as is done in, e.g., the OFC model of SOC [43].

As long as there are no observable differences for experimentally relevant system sizes, we will here not distinguish between *quasi-critical* and *critical*, i.e., truly scale-free behavior. Instead, we focus on the question of whether or not dissipation modifies the universality class in the spreading process of Rydberg facilitation, i.e., if the critical exponents τ_μ in Eq. (11) are modified. In particular, we will explore by numerial simulations if dissipation acts as a relevant perturbation in the renormalization sense. Since our atom loss mechanism is conceptually very similar to that of the generalized epidemic process (GEP) or, more generally, of dynamical percolation (DyP), the presence of dissipation may change the critical behavior to that of the DyP universality class, and we will compare our results with the corresponding predictions. In the GEP and DyP models, an individual's probability to be infected for the first time and that of all subsequent infections differ, the latter being set to zero in the extreme (GEP) case, which is referred to as perfect immunization. For the more general case of reduced repeated infection probability, the phase transition is part of the DyP universality class [17,44]. The three-dimensional case of DyP is characterized by the critical exponents [17]

$$\beta = 0.417, \quad \nu_\parallel = 1.169, \quad \nu_\perp = 0.875, \tag{12}$$

which via (10) then result in

$$\tau_a \approx 1.159, \quad \tau_s \approx 1.123, \quad \tau_t \approx 1.357. \tag{13}$$

In our model of Rydberg facilitation, dissipation is controlled by the b parameter. The value $b = 0$ corresponds to a dynamics where all Rydberg atoms return to the ground state after an exponentially distributed time. The value $b = 1$, however, leads to the guaranteed irreversible loss of this atom from a Rydberg state.

To address the effect of dissipation, we simulate the avalanches in the system with varying values of $b > 0$. Generically, we find a power law scaling over 1–2 orders of magnitude truncated by an exponential cutoff function, Eq. (11). We extract the power-law exponents and perform finite-size extrapolations. The result can be seen in Fig. 9. We observe that at $v = 0$ for loss parameters $b < 0.01$, we do not find a difference in the values of the exponents larger than our uncertainty. For larger b, the found exponents diminish in magnitude, especially the time exponent. For the case of $v = 1.37 r_f \gamma$, which is approximately the gas velocity in the experiment, we find that the avalanche exponents follow a nonmonotonous behavior of increase for smaller b and decreasing in magnitude again for larger b. Importantly, this implies that the avalanche exponents found in the experiment, which we also show in Fig. 9, do not incur a significant additional systematic error based on nonvanishing b values. In Fig. 9 we also show the predicted values for DyP. We observe that neither the simulated nor the experimentally measured values agree with those of DyP, showing that despite the conceptual similarity, Rydberg facilitation cannot be simply pictured as an epidemic spreading with immunization. We have checked that this deviation does not result from the network structure set by the random atom positions in a gas by

repeating our avalanche simulations on a regular 2D lattice of atoms with nearest-neighbor facilitation. Here, we also find no agreement with DyP exponents for $b \to 1$. We speculate that the difference might be found in the infection mechanism: In lattice models of DyP, an infected site passes on the infection to adjacent sites with a given probability, but decays after a single step of discrete time [44,45], whereas in our model, both infection and decay occur probabilistically according to certain rates.

V. CONCLUSION

We studied the critical properties of excitation growth in a gas of atoms under conditions of Rydberg facilitation, which represents an experimentally accessible model system for a spreading process on a random and dynamical network. In particular we determined the power-law exponents of the distribution of avalanches at the critical point of the absorbing-state phase transition (ASPT) from both numerical simulations and experimental measurements. These exponents can be related to the full set of critical exponents of the nonequilibrium phase transition and thus uniquely determine the universality class Eq. (10). In a previous theoretical work we have provided numerical evidence that with increasing rms velocity of the atoms in the gas, the character of the ASPT smoothly changes from directed percolation (DP) universality through different classes of anomalous directed percolation (ADP) to eventually mean-field (MF) behavior, which also explained previous experimental observations [24]. The velocity-dependent crossover was interpreted using a phenomenological model that mapped the Rydberg facilitation in the gas of moving atoms, resembling a dynamic network to an excitation spreading process on a random static network with Lévy-flight tails in the distribution of excitation distances [28]. Our simulations together with experimental results confirm that the avalanche distribution exponents follow the predictions obtained from the phenomenological model in Ref. [28] using the mapping relations (10) combined with previous results on the velocity dependence of the Lévy-flight parameter at the ASPT. Furthermore, our work has given experimental evidence of ADP universality.

We also investigated the network structure and its effects on the SOC mechanism. Since SOC on dynamical networks has been little researched and is as of yet poorly understood, we first characterize the dynamical properties of the underlying network structure of atoms in mutual facilitation distance as a function of gas velocity and quantify the number of dynamical connections. Secondly, we investigated the influence of dissipation, important for the SOC, on the critical behavior. For the frozen gas, we first verified that the Erdős-Rényi character of the network is unaffected by decay. We then analyzed the influence of decay on the critical scaling in the DP and ADP regimes. While we cannot make any claims about the presence or absence of true critical behavior over arbitrary time and length scales, the observed power laws in the avalanche distributions over extended parameter ranges even in the presence of losses are consistent with at least quasi-critical behavior. The question we addressed instead was whether losses modify the universality class of the ASPT in Rydberg facilitation, which could be the case if dissipation was a relevant perturbation in the renormalization sense. For a frozen gas we find that below a minimal dissipation probability we cannot detect a measurable influence on the scaling exponents. At stronger dissipation we see that the avalanche exponents are slightly reduced in magnitude. However, despite the conceptual similarities, we do not obtain exponents belonging to the dynamical percolation (DyP) universality class.

ACKNOWLEDGMENTS

The authors thank Fabian Isler for fruitful discussions. Financial support from the DFG through SFB TR 185, Project No. 277625399, is gratefully acknowledged. The authors also thank the Allianz für Hochleistungsrechnen (AHRP) for giving us access to the Elwetritsch HPC Cluster. This work was also supported by the Max Planck Graduate Center with the Johannes Gutenberg-Universität Mainz (MPGC) and the Quantum Initiative Rhineland-Palatinate (QUIP) and the Research Initiative Quantum Computing for Artificial Intelligence QC-AI. W.R. acknowledges support by the German Ministry of Education and Research (BMBF) for BIFOLD (01IS18037A).

S.O. performed the numerical calculations and the analysis of critical exponents with support from D.B. The experiment was performed by J.B., P.M., and D.B., guided by T.N., and H.O.; W.R. and J.S.O. helped in numerical implementation and optimization. J.S.O. additionally helped in supervising the theoretical work. M.F. and T.N. conceived the project and supervised the theoretical (M.F.) and experimental parts (T.N.) of the project, respectively. S.O., D.B., and M.F. wrote the initial version of the paper. All authors discussed the results and contributed to the writing of the final manuscript.

DATA AVAILABILITY

The data that support the findings of this article are openly available [46].

APPENDIX A: RATE EQUATION MODELING

All numerical data is obtained using fixed-time-step Monte Carlo simulations [47] of classical rate equations in the high dephasing limit. It has been shown that in this limit dynamics become effectively classical and can therefore be described by classical Monte Carlo simulations to a high degree of accuracy [33].

For atom i, the excitation probability is given by the projection operator onto the Rydberg state $|R\rangle_i$, i.e., $\hat{n}_i = |R\rangle_i \langle R|_i$. Using the Lindblad master equation, given by Eq. (1), we can formulate a set of differential equations for the ground state $|G\rangle_i$, Rydberg state $|R\rangle_i$, and inert state $|0\rangle_i$ of the ith atom. After adiabatic elimination of coherences, e.g., $\frac{d}{dt}\sigma_i^{gr} = 0$, (where $\sigma^{gr} = |G\rangle\langle R|$), we receive the rate equations [22,34]

$$\frac{d}{dt}p_r^{(i)} = -(\gamma_{\text{stim}} + \gamma_{\text{spont}})p_r^{(i)} + \gamma_{\text{stim}}p_g^{(i)}, \tag{A1}$$

$$\frac{d}{dt}p_g^{(i)} = -\gamma_{\text{stim}}p_g^{(i)} + (\gamma_{\text{stim}} + (1-b)\gamma_{\text{spont}})p_r^{(i)}, \tag{A2}$$

$$\frac{d}{dt}p_0^{(i)} = b\gamma_{\text{spont}}p_r^{(i)}. \tag{A3}$$

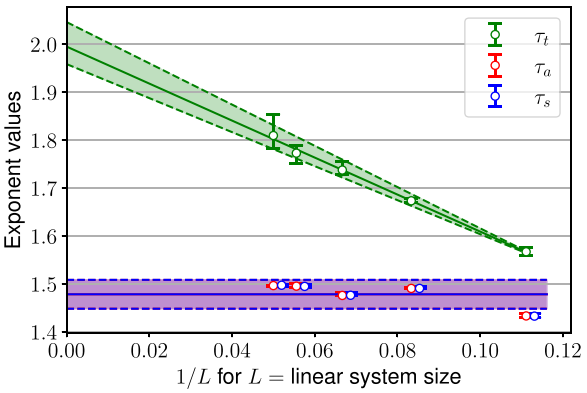

FIG. 10. Finite-size expansion of the avalanche exponents. The shaded area corresponds to the uncertainty interval. Size values are shifted slightly along the x axis for better visibility.

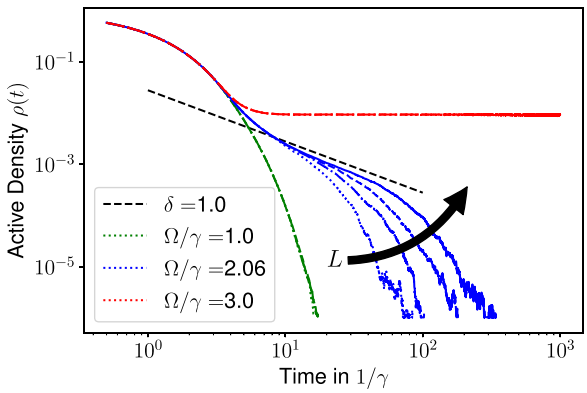

FIG. 11. Finite-size expansion of the active density decay method of finding Ω_c for $v = 10 r_f \gamma$. For all values of Ω, we show the averaged decay data for $L \in \{5, 7, 9\} r_f$; for $\Omega/\gamma = 2.06$ we also show $L = 12 r_f$. The linestyles with increasing system size are: dotted, dash-dotted, dashed, and solid.

Here, γ_{spont} corresponds to the spontaneous decay rate and γ_{stim} corresponds to the stimulated (de)excitation rate. Explicitly, the stimulated rate reads

$$\gamma_{\text{stim}} = \frac{2\Omega^2 \gamma_\perp}{\gamma_\perp^2 + \Delta^2 \left(\sum_{\substack{j \neq i \\ j \in \Sigma}} \frac{r_f^6}{r_{ij}^6} - 1 \right)^2}, \tag{A4}$$

where Σ corresponds to the subset of atoms in the Rydberg state.

We initiate N atoms with random positions in a cubic simulation box with length L and periodic boundary conditions. Velocities are sampled from the Maxwell-Boltzmann distribution, i.e., a Gaussian in each direction, with the most probable velocity v. Furthermore, we dynamically adjust the (fixed) time-step length depending on the facilitation rate with $\Gamma_f \, dt = \frac{1}{10}$. In order to receive good avalanche fits, we use approximately 200 000 trajectories per parameter set.

APPENDIX B: FINITE-SIZE EXPANSION OF AVALANCHE DATA

All of the simulation exponent values reported in this paper were obtained using a system size extrapolation. We fit a linear function $f(1/L)$, where L is the linear system size, to the exponent values for different system sizes and then extrapolate to $f(0)$. In Fig. 10 we show the extrapolation for the case of $v = 1.37 r_f \gamma$ in the ADP phase. For the time exponent we see a clear finite-size scaling with an increasing value for larger systems, whereas the area and size exponents do not show a clear trend over system size as well as a much smaller variation. The shaded areas correspond to the uncertainty region.

APPENDIX C: DETERMINING THE CRITICAL POINT

1. Numerical simulations

Finding the correct critical point Ω_c is essential in obtaining power-law distributed avalanches. We determine Ω_c in our numerical simulations by starting from the fully inverted state (all atoms in the Rydberg state) and considering the decay process as a function of the system size. In the absorbing phase, the decay is exponential and shows no strong dependence on system size. In the active phase, the Rydberg density approaches a constant. For values of Ω close to the critical point, a regime with power-law decay emerges for intermediate time scales, where the precise value of Ω_c is then obtained by fitting a power-law function with the exponent $\delta = \frac{\beta}{\nu_\parallel}$ to increasing system sizes L as shown in Fig. 11. Note that for the absorbing as well as the active case the curves for all system sizes lie on top of each other. Also see Ref. [38] for more details. We find $\Omega_c/\gamma \approx 3.40$ for the frozen gas, $\Omega_c/\gamma \approx 2.325$ for the ADP regime ($v = 1.37 r_f \gamma$), and $\Omega_c/\gamma \approx 2.06$ for the mean-field regime ($v = 10 r_f \gamma$).

2. Experimental data

The extracted exponents of the power-law distributed avalanches strongly depend on the time windows in which they are evaluated. It is a challenging task to determine the correct point in time at which the critical point is reached. In the active phase, the system typically forms a single large cluster of Rydberg excitations where the total number of excited atoms is effectively limited by the size of the system. In Fig. 12 we show histograms of the count numbers in a single evaluation bin for different time windows. As the number of ions in a fixed time t_{bin} is proportional to the number of Rydberg atoms times the decay rate, this can be understood as a measure for the activity of the system. In the active phase, which is our starting point, the histograms show a characteristic activity bump for large counts. We estimate that the active phase ends when the distribution shows no residuals of such an activity bump clearly visible in the first evaluation frame. In our experiment, we estimate that this is the case between 8 and 13 ms, i.e., time window centers of 9.5 and 11.5 ms.

We note that other, more indirect ways to estimate the critical point are possible, e.g., by exploiting scaling relations of avalanche shapes [48]. Moreover, the critical point may be reached after slightly different times in each individual experimental realization, given that the loss process is stochastic.

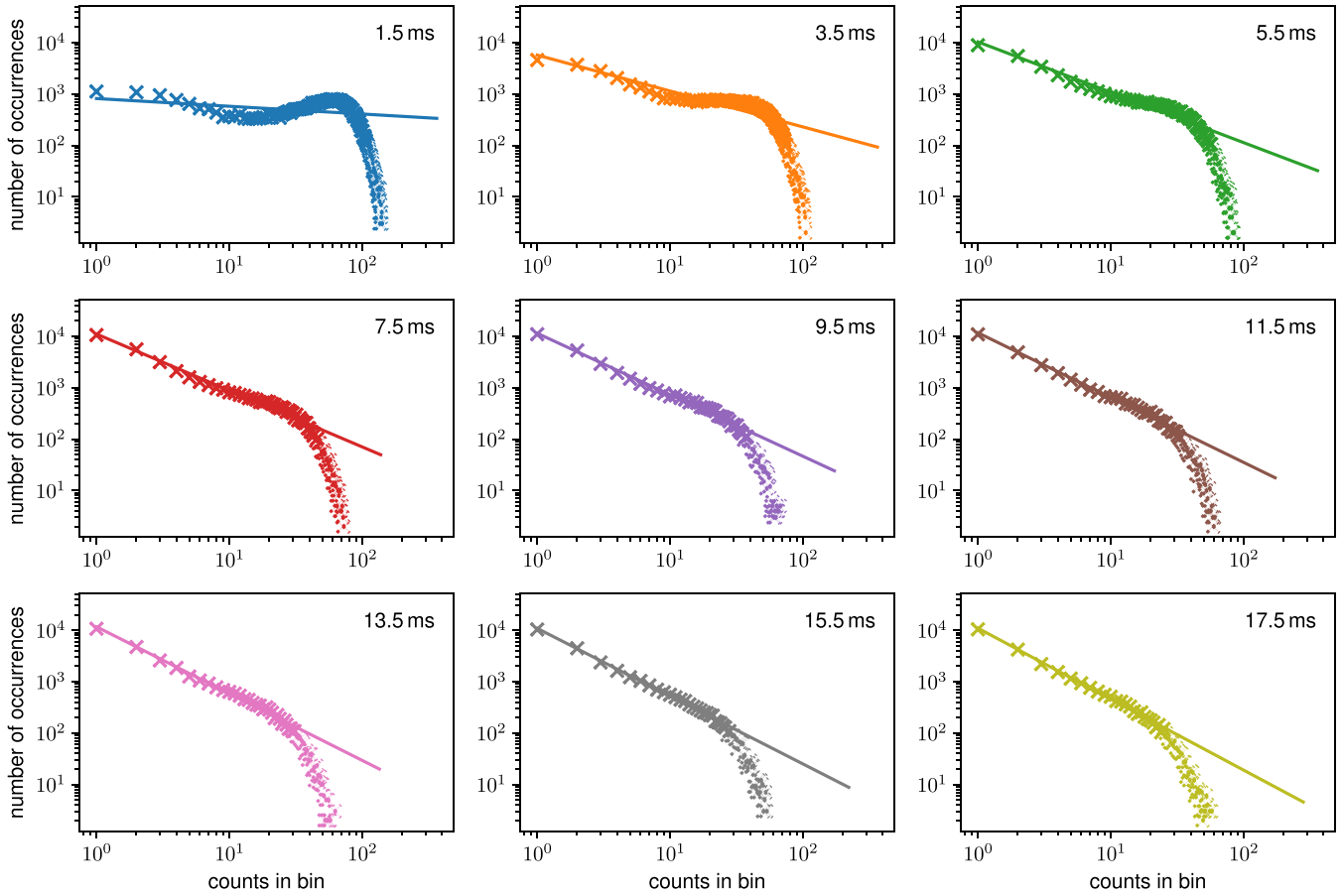

FIG. 12. The activity distribution of the experimental system at different time intervals. In each subplot, the activitiy distribution for a different time interval of $\Delta t = 3$ ms is shown, centered as indicated in the corner of the plot. The distribution of count numbers in 50-µs bins is shown. The fitted lines serve as a guide to the eye to evaluate whether the distribution is active. For early times up until the interval of 6–9 ms we find a "bump" at large activity sizes, which is indicative of the active phase. We estimate that in the subsequent time windows of 8–13 ms the critical point is reached.

[1] P. Bak, C. Tang, and K. Wiesenfeld, Self-organized criticality: An explanation of the 1/*f* noise, Phys. Rev. Lett. **59**, 381 (1987).

[2] P. Bak, C. Tang, and K. Wiesenfeld, Self-organized criticality, Phys. Rev. A **38**, 364 (1988).

[3] C. Tang and P. Bak, Critical exponents and scaling relations for self-organized critical phenomena, Phys. Rev. Lett. **60**, 2347 (1988).

[4] N. W. Watkins, G. Pruessner, S. C. Chapman, N. B. Crosby, and H. J. Jensen, 25 years of self-organized criticality: Concepts and controversies, Space Sci. Rev. **198**, 3 (2016).

[5] A. Sornette and D. Sornette, Self-organized criticality and earthquakes, Europhys. Lett. **9**, 197 (1989).

[6] E. T. Lu and R. J. Hamilton, Avalanches and the distribution of solar flares, Astrophysical Journal, Part 2-Letters **380**, L89 (1991).

[7] M. J. Aschwanden, N. B. Crosby, M. Dimitropoulou, M. K. Georgoulis, S. Hergarten, J. McAteer, A. V. Milovanov, S. Mineshige, L. Morales, N. Nishizuka *et al.*, 25 years of self-organized criticality: solar and astrophysics, Space Sci. Rev. **198**, 47 (2016).

[8] D. Plenz, T. L. Ribeiro, S. R. Miller, P. A. Kells, A. Vakili, and E. L. Capek, Self-organized criticality in the brain, Front. Phys. **9**, 639389 (2021).

[9] J. Hesse and T. Gross, Self-organized criticality as a fundamental property of neural systems, Front. Syst. Neurosci. **8**, 166 (2014).

[10] S. S. Manna, Two-state model of self-organized criticality, J. Phys. A: Math. Gen. **24**, L363 (1991).

[11] B. Drossel and F. Schwabl, Self-organized critical forest-fire model, Phys. Rev. Lett. **69**, 1629 (1992).

[12] Z. Olami, H. J. S. Feder, and K. Christensen, Self-organized criticality in a continuous, nonconservative cellular automaton modeling earthquakes, Phys. Rev. Lett. **68**, 1244 (1992).

[13] F. Caruso, V. Latora, A. Pluchino, A. Rapisarda, and B. Tadić, Olami-Feder-Christensen model on different networks, Eur. Phys. J. B **50**, 243 (2006).

[14] M. Dottori and G. Fabricius, Sir model on a dynamical network and the endemic state of an infectious disease, Physica A **434**, 25 (2015).

[15] S. Lise and M. Paczuski, Nonconservative earthquake model of self-organized criticality on a random graph, Phys. Rev. Lett. **88**, 228301 (2002).

[16] J. A. Bonachela and M. A. Munoz, Self-organization without conservation: true or just apparent scale-invariance? J. Stat. Mech. (2009) P09009.

[17] M. Henkel, H. Hinrichsen, and S. Lübeck, *Non-Equilibrium Phase Transitions*, 1st ed., Theoretical and Mathematical Physics (Springer Science+Business Media, Dordrecht, 2008), Vol. 1.

[18] K. A. Takeuchi, M. Kuroda, H. Chaté, and M. Sano, Directed percolation criticality in turbulent liquid crystals, Phys. Rev. Lett. **99**, 234503 (2007).

[19] A. Browaeys and T. Lahaye, Many-body physics with individually controlled Rydberg atoms, Nat. Phys. **16**, 132 (2020).

[20] M. Saffman, T. G. Walker, and K. Mølmer, Quantum information with Rydberg atoms, Rev. Mod. Phys. **82**, 2313 (2010).

[21] C. S. Adams, J. D. Pritchard, and J. P. Shaffer, Rydberg atom quantum technologies, J. Phys. B: At. Mol. Opt. Phys. **53**, 012002 (2019).

[22] D. Brady and M. Fleischhauer, Mean-field approach to Rydberg facilitation in a gas of atoms at high and low temperatures, Phys. Rev. A **108**, 052812 (2023).

[23] T. Wintermantel, M. Buchhold, S. Shevate, M. Morgado, Y. Wang, G. Lochead, S. Diehl, and S. Whitlock, Epidemic growth and Griffiths effects on an emergent network of excited atoms, Nat. Commun. **12**, 103 (2021).

[24] S. Helmrich, A. Arias, G. Lochead, T. Wintermantel, M. Buchhold, S. Diehl, and S. Whitlock, Signatures of self-organized criticality in an ultracold atomic gas, Nature (London) **577**, 481 (2020).

[25] M. Marcuzzi, E. Levi, W. Li, J. P. Garrahan, B. Olmos, and I. Lesanovsky, Non-equilibrium universality in the dynamics of dissipative cold atomic gases, New J. Phys. **17**, 072003 (2015).

[26] R. Gutiérrez, C. Simonelli, M. Archimi, F. Castellucci, E. Arimondo, D. Ciampini, M. Marcuzzi, I. Lesanovsky, and O. Morsch, Experimental signatures of an absorbing-state phase transition in an open driven many-body quantum system, Phys. Rev. A **96**, 041602 (2017).

[27] I. Lesanovsky and J. P. Garrahan, Out-of-equilibrium structures in strongly interacting Rydberg gases with dissipation, Phys. Rev. A **90**, 011603 (2014).

[28] D. Brady, S. Ohler, J. Otterbach, and M. Fleischhauer, Anomalous directed percolation on a dynamic network using Rydberg facilitation, Phys. Rev. Lett. **133**, 173401 (2024).

[29] G. Lindblad, On the generators of quantum dynamical semigroups, Commun. Math. Phys. **48**, 119 (1976).

[30] W. Li, C. Ates, and I. Lesanovsky, Nonadiabatic motional effects and dissipative blockade for Rydberg atoms excited from optical lattices or microtraps, Phys. Rev. Lett. **110**, 213005 (2013).

[31] T. Schlegel, E. Konstantinidou, M. Fleischhauer, and D. Brady arXiv:2505.09314.

[32] C. Ates, T. Pohl, T. Pattard, and J. Rost, Strong interaction effects on the atom counting statistics of ultracold Rydberg gases, J. Phys. B: At. Mol. Opt. Phys. **39**, L233 (2006).

[33] E. Levi, R. Gutiérrez, and I. Lesanovsky, Quantum non-equilibrium dynamics of Rydberg gases in the presence of dephasing noise of different strengths, J. Phys. B: At. Mol. Opt. Phys. **49**, 184003 (2016).

[34] D. Brady, J. Bender, P. Mischke, S. Ohler, T. Niederprüm, H. Ott, and M. Fleischhauer, Griffiths phase in a facilitated Rydberg gas at low temperatures, Phys. Rev. Res. **6**, 013052 (2024).

[35] P. Erdős and A. Rényi, On the evolution of random graphs, Publ. math. inst. hung. acad. sci **5**, 17 (1960).

[36] H. Hinrichsen and M. Howard, A model for anomalous directed percolation, Eur. Phys. J. B **7**, 635 (1999).

[37] M. A. Munoz, R. Dickman, A. Vespignani, and S. Zapperi, Avalanche and spreading exponents in systems with absorbing states, Phys. Rev. E **59**, 6175 (1999).

[38] M. A. Munoz, R. Juhász, C. Castellano, and G. Ódor, Griffiths phases on complex networks, Phys. Rev. Lett. **105**, 128701 (2010).

[39] H. Hinrichsen, Non-equilibrium phase transitions with long-range interactions, J. Stat. Mech. (2007) P07006.

[40] S. Manna, Large-scale simulation of avalanche cluster distribution in sand pile model, J. Stat. Phys. **59**, 509 (1990).

[41] S. Lübeck and K. Usadel, Numerical determination of the avalanche exponents of the Bak-Tang-Wiesenfeld model, Phys. Rev. E **55**, 4095 (1997).

[42] K. B. Lauritsen, S. Zapperi, and H. E. Stanley, Self-organized branching processes: Avalanche models with dissipation, Phys. Rev. E **54**, 2483 (1996).

[43] S. Lise and H. J. Jensen, Transitions in nonconserving models of self-organized criticality, Phys. Rev. Lett. **76**, 2326 (1996).

[44] P. Grassberger, H. Chaté, and G. Rousseau, Spreading in media with long-time memory, Phys. Rev. E **55**, 2488 (1997).

[45] A. Jiménez-Dalmaroni and H. Hinrichsen, Epidemic processes with immunization, Phys. Rev. E **68**, 036103 (2003).

[46] S. Ohler, D. Brady, P. Mischke, J. Bender, H. Ott, T. Niederprüm, W. Ripken, J. S. Otterbach, and M. Fleischhauer, Nonequilibrium universality of Rydberg-excitation spreading on a dynamic network [dataset] RPTU Kaiserslautern-Landau (2025), 10.26204/data/9.

[47] V. R. Barlett, J. Bigeón, M. Hoyuelos, and H. Mártin, Differences between fixed time step and kinetic Monte Carlo methods for biased diffusion, J. Comput. Phys. **228**, 5740 (2009).

[48] J. P. Sethna, K. A. Dahmen, and C. R. Myers, Crackling noise, Nature (London) **410**, 242 (2001).